*Neuroscience*

*The Journal of Physiology*

# Disrupted hippocampal sharp-wave ripple-associated spike dynamics in a transgenic mouse model of dementia

Jonathan Witton[1], Lydia E. Staniaszek[2], Ullrich Bartsch[1], Andrew D. Randall[1,2], Matthew W. Jones[1] and Jonathan T. Brown[1,2]

[1] *School of Physiology and Pharmacology, University of Bristol, University Walk, Bristol, BS8 1TD, UK*
[2] *Institute of Biomedical and Clinical Sciences, University of Exeter Medical School, University of Exeter, Hatherly Laboratories, Prince of Wales Road, Exeter, EX4 4PS, UK*

**Key points**

- High frequency (100–250 Hz) neuronal oscillations in the hippocampus, known as sharp-wave ripples (SWRs), synchronise the firing behaviour of groups of neurons and play a key role in memory consolidation.
- Learning and memory are severely compromised in dementias such as Alzheimer's disease; however, the effects of dementia-related pathology on SWRs are unknown.
- The frequency and temporal structure of SWRs was disrupted in a transgenic mouse model of tauopathy (one of the major hallmarks of several dementias).
- Excitatory pyramidal neurons were more likely to fire action potentials in a phase-locked manner during SWRs in the mouse model of tauopathy; conversely, inhibitory interneurons were less likely to fire phase-locked spikes during SWRs.
- These findings indicate there is reduced inhibitory control of hippocampal network events and point to a novel mechanism which may underlie the cognitive impairments in this model of dementia.

**Abstract**   Neurons within the CA1 region of the hippocampus are co-activated during high frequency (100–250 Hz) sharp-wave ripple (SWR) activity in a manner that probably drives synaptic plasticity and promotes memory consolidation. In this study we have used a transgenic mouse model of dementia (rTg4510 mice), which overexpresses a mutant form of tau protein, to examine the effects of tauopathy on hippocampal SWRs and associated neuronal firing. Tetrodes were used to record simultaneous extracellular action potentials and local field potentials from the dorsal CA1 pyramidal cell layer of 7- to 8-month-old wild-type and rTg4510 mice at rest in their home cage. At this age point these mice exhibit neurofibrillary tangles, neurodegeneration and cognitive deficits. Epochs of sleep or quiet restfulness were characterised by minimal locomotor activity and a low theta/delta ratio in the local field potential power spectrum. SWRs detected off-line were significantly lower in amplitude and had an altered temporal structure in rTg4510 mice. Nevertheless, the average frequency profile and duration of the SWRs were relatively unaltered. Putative interneurons displayed significantly less temporal and phase locking to SWRs in rTg4510 mice, whilst putative pyramidal neurons showed increased temporal and phase locking to SWRs. These findings indicate there is reduced inhibitory control of hippocampal network events and point to a novel mechanism which may contribute to impairments in memory consolidation in this model of dementia.

**Corresponding author** J. Brown: Institute of Biomedical and Clinical Sciences, University of Exeter Medical School, University of Exeter, Hatherly Laboratories, Prince of Wales Road, Exeter, Devon, EX4 4PS, UK.  Email: j.t.brown@exeter.ac.uk

**Abbreviations**   AD, Alzheimer's disease; CCK, cholecystokinin; FTD, fronto-temporal dementia; LFP, local field potential; PV+, parvalbumin positive; QR, quiet restfulness; SD, standard deviation; SWR, sharp-wave ripple; WT, wild-type.

## Introduction

Neuronal spiking activity is coordinated by synchronous membrane potential oscillations, which occur at a wide range of frequency scales (Buzsáki & Draguhn, 2004). High frequency oscillations (100–250 Hz) in the hippocampus drive the synchronous co-activation of local populations of pyramidal neurons and interneurons (Ylinen *et al.* 1995; Csicsvari *et al.* 1999; Klausberger & Somogyi, 2008). In rodents and humans, brief periods (30–100 ms) of high frequency oscillations, or 'ripples', co-occur with large extracellular voltage deflections (known collectively as sharp-wave ripples or SWRs) during periods of sleep and quiet restfulness (Buzsáki *et al.* 1992; Clemens *et al.* 2007; Le Van Quyen *et al.* 2008). The coordinated firing that occurs with SWRs is thought to play an important role in driving Hebbian synaptic plasticity (Sadowski *et al.* 2011). Hippocampal place cells are reactivated in a compressed time frame during SWRs in a manner that recapitulates spatial experience (Nádasdy *et al.* 1999; Lee & Wilson, 2002; Davidson *et al.* 2009; Karlsson & Frank, 2009). This process (known as replay) is thought to play a critical role in consolidation of spatial memory.

The generation and temporal structure of SWR events relies on a precisely co-ordinated interplay between excitatory and inhibitory synaptic activity (Cutsuridis & Taxidis, 2013). Of the wide variety of GABAergic interneurons found within the hippocampus (Klausberger & Somogyi, 2008), several alter their firing rate during SWRs. For example, parvalbumin expressing (PV+) basket cells and bi-stratified cells both increase their firing rate during or immediately prior to SWRs, whilst axo-axonic cells decrease their firing rate (Klausberger *et al.* 2003, 2004). In contrast, cholecystokinin (CCK)-positive interneurons typically do not alter their firing patterns during SWR events (Klausberger *et al.* 2005). The specific roles for each of these cell types in generating and shaping SWRs is not fully understood, although a number of models have been proposed (Traub & Bibbig, 2000; Cutsuridis & Taxidis, 2013; Simon *et al.* 2014; Stark *et al.* 2014). Nevertheless, it is clear that interneurons which target the perisomatic region of pyramidal cells play a key role both in generating SWRs (Ellender *et al.* 2010) and controlling pyramidal neuron recruitment (Bähner *et al.* 2011).

Dementias such as Alzheimer's disease (AD) and fronto-temporal dementia (FTD) result in severe cognitive impairments. In part, these impairments arise from extensive neurodegeneration which characterises the pathology of these diseases. However, there is a growing understanding that deficits in synaptic transmission and plasticity may also contribute to the symptoms of dementia (Selkoe, 2002). Indeed, there is now a substantial body of evidence (garnered largely from experiments in transgenic mice) that the various pathological features of dementia (e.g. $\beta$-amyloid deposition, tau accumulation, etc.) can produce a number of different neurophysiological phenotypes (Randall *et al.* 2010). In particular, there is a growing literature suggesting that neuronal networks are hyperexcitable in mouse models and clinical dementia (Palop *et al.* 2007; Busche *et al.* 2008; Noebels, 2011; Corbett *et al.* 2013). That said, there is very little published literature pertaining to the effects of dementia-like pathologies on high frequency SWRs. Tauopathy is a pathological hallmark of several dementias, including AD. Here, we have examined SWR activity and associated cellular activity in behaving transgenic mice which over-express a mutant (P301L) form of the microtubule associated protein tau (rTg4510 mice; Ramsden *et al.* 2005; Santacruz *et al.* 2005). rTg4510 mice develop neurofibrillary tangles and neurodegeneration associated with cognitive behavioural deficits, in an age-dependent manner (Ramsden *et al.* 2005; Spires *et al.* 2006). We have used rTg4510 and wild-type (WT) littermate mice at an age point (7–8 months) at which neurodegeneration is well established (Ramsden *et al.* 2005; Spires *et al.* 2006), to determine the effects of degenerative processes on SWR-associated network dynamics.

## Methods

### Ethical approval

All procedures were carried out in accordance with the UK Animals (Scientific Procedures) Act 1986 and EU Directive 2010/63/EU. Furthermore, all experimental procedures were reviewed by the University of Bristol Ethical Review Group.

### Experimental animals

rTg4510 mice and their wild-type (WT) littermates (Charles River, CT, USA) were used in this study.

These mice transgenically express human four-repeat tau, containing the P301L mutation, under control of a tetracycline operon-responsive element (SantaCruz *et al.* 2005). Mice were bred on a mixed 129S6 × FVB/N genetic background. Genotypes were confirmed using PCR analysis. Mice were weaned at 3 weeks of age and housed according to gender and litter on a 12–12 h light–dark cycle with *ad libitum* access to food and water. 7- to 8-month-old male mice were used in experiments and were housed singly for at least 2 weeks prior to experiments. At this age, rTg4510 mice have extensive tau pathology in both cortex and hippocampus (Ramsden *et al.* 2005). These mice also show cortical atrophy at ages above 5.5 months (Ramsden *et al.* 2005); by 7 months the CA1 region may have lost approximately 50% of neurons and brain weight is approximately 15% lower than that of age-matched WT mice (Spires *et al.* 2006). Thus, at the age point chosen for this study, significant neurodegeneration has occurred. Furthermore, cognitive dysfunction (as measured using the Morris water maze) becomes apparent at 4.5 months of age (Ramsden *et al.* 2005), while a recent study using this mouse line identified disrupted hippocampal theta oscillations and spatially modulated firing of putative place cells (Cheng & Ji, 2013).

## Surgery

Mice were implanted with bespoke microdrives which contained four independently movable tetrodes. Tetrodes were fabricated from four individual 12.5 $\mu$m Formvar insulated tungsten wires (California Fine Wire, CA, USA), which were twisted and heat bonded together. Tetrodes were blunt cut to similar lengths using SuperCut scissors (World Precision Instruments, Sarasota, FL, USA) and gold plated to reduce the impedance to 200–300 k$\Omega$.

Mice were initially anaesthetised using inhalational anaesthetic (isoflurane, 4%) and fixed in a stereotaxic frame (Stoelting, Dublin, Ireland). Anaesthesia was then reduced to and maintained at 1–2% isoflurane during surgery. To anchor the microdrive, seven watchmakers' screws were inserted into the skull: two rostral to bregma, two over left parietal cortex, one over right parietal cortex, and two caudal to lambda. A 1 mm$^2$ craniotomy was made over right parietal cortex and tetrodes were implanted into the brain at stereotaxic coordinates (mm, relative to bregma): AP = −2.0–2.2; ML = +1.5–2.0. Tetrodes were implanted to a depth of 0.5–0.7 mm, measured from the brain surface, and sealed off using a 70% paraffin wax–30% mineral oil mixture. Silver ground and reference wires (World Precision Instruments) were connected to the anchor screws overlying the cerebellum. Gentamycin impregnated bone cement was used to anchor the microdrive to the skull.

## *In vivo* electrophysiology data acquisition

After 1 week post-operative recovery, tetrodes were advanced by ∼30–60 $\mu$m day$^{-1}$ until neurophysiological signatures characteristic of the CA1 pyramidal cell layer could be identified (i.e. ripple oscillations, theta modulation, complex spiking cells). one of the four tetrodes was placed either in the white matter dorsal to hippocampus or in a 'silent' region in the deep layers of cortex and was used as a local reference electrode. Screening sessions were performed in the animal's home cage to provide epochs of both resting (ripple-state) and exploratory (theta-state) behaviour.

Tetrodes were used to record both single units and local field potentials (LFPs). Signals were recorded by tethering the implanted microdrive to a Cheetah 32 analog recording system (Neuralynx, Bozeman, MT, USA) via a HS-18 unity gain headstage (Neuralynx). Signals were digitised using Cheetah 5 data acquisition software (Neuralynx). Units were threshold triggered at 50 $\mu$V, band-pass filtered between 400–6000 Hz and digitised at 30 kHz. LFPs were band-pass filtered between 1–475 Hz and sampled continuously at 2 kHz. LFPs were acquired from all three hippocampal tetrodes, with one of these signals selected for analyses. Efforts were made to ensure consistent neuro-anatomical placement of the LFP electrode across animals, based on the *ex vivo* histology. Units were referenced to the local reference tetrode whereas LFPs were referenced to the cerebellar ground screw. The latter was to prevent parietal or volume conducted hippocampal network activity detected on the local reference from biasing the hippocampal LFP. Two light-emitting diodes on the headstage and an overhead video camera were used to continuously track the animal's location at 25 Hz. The video acquisition was time locked to the electrophysiology acquisition.

Experiments began once isolated complex spiking cells were identified. Experiments were performed in the light phase of a 12–12 h light–dark cycle. Animals were placed in their home cages whilst tethered to the recording device and neural activity was recorded for >60 min. Acoustic noise was kept to a minimum to encourage the mice to sleep. At the end of each recording session tetrodes were regularly adjusted to optimise their placement for the following day.

At the end of all experimental procedures, mice received an overdose of sodium pentoparbital (Euthetal) and electrolytic lesions were made at the tetrode tips by delivering a 30 $\mu$A anodal current for 10 s. Mice were then transcardially perfused with 0.1 M PBS followed by 4% v/v formaldehyde in 0.1 M PBS. Approximately 2 h after perfusion, tetrodes were retracted and the brain was removed from the skull. Brains were post-fixed in 4% formaldehyde for a minimum of 24 h and cryoprotected in 30% w/w sucrose in 0.1 M PBS for ∼ 48 h. Brains were

cut into 50 $\mu$m coronal sections using a freezing micro-tome, mounted onto slides, and stained using thionin blue. Confirmation of the final tetrode positions was performed at ×2.5 magnification on a light microscope using trans-mitted bright-field illumination.

### *In vivo* electrophysiology data analysis

All analyses were performed in Matlab (Mathworks, Natick, MA, USA). Animal position and running speed were estimated based on the tracking of the headstage LEDs. LFP recordings from one of the s. pyramidale located tetrodes were binned into 30 s epochs and a multi-taper (number of tapers = 10) Fourier power analysis performed using the Chronux tool box (Bokil *et al.* 2010). The ratio of the power in the delta (1–3 Hz) and theta (6–12 Hz) frequency bands was calculated for each epoch. Time epochs in which the animals were considered to be asleep or in a state of quiet restfulness (QR) were identified as those in which: (1) average movement speed was <4 cm s$^{-1}$ and (2) the theta/delta ratio in the hippocampal LFP power was <4 (see Fig. 1*A*).

Within the identified sleep/QR epochs, individual SWR events were detected from the LFP. The LFP was trans-formed by (1) band-pass filtering (100–250 Hz); (2) rectifying; and (3) *Z*-normalisation. A cubic spline inter-polation between the resulting peaks resulted in the 'ripple envelope'. Individual SWR events were detected as peak deviations of the mean envelope of greater than 4 standard deviations (SD) of the mean band-pass filtered LFP. The start and end points of the SWR event were determined as the points either side of the peak which fell below 2 SDs. Individual events shorter than 30 ms and longer than 1 s in duration and events which were <100 $\mu$V in amplitude were excluded from further analysis. Separate events that occurred within 10 ms of each other were merged and reassessed against the above criteria (Phillips *et al.* 2012).

To assess the temporal dynamics of SWR events, the onset times of the individual SWR events were used to calculate the SWR-triggered short-time Fourier trans-form of wide-band (80–400 Hz) filtered LFP (Hamming window length 30 samples, overlap 29 samples). The individual spectrograms were normalised (to total power within the time-frequency window) and averaged within a recording session.

Single units were isolated off-line by clustering the spikes using MClust−4.0 (A. D. Redish *et al.*; available at http://redishlab.neuroscience.umn.edu/MClust/MClust.html). Cluster quality inclusion criteria were set at iso-lation distance >15 and L-ratio <0.35 (Schmitzer-Torbert *et al.* 2005). Putative pyramidal and interneurons were classified according to standard waveform and firing rate analyses: units with a mean overall firing rate ≤5 Hz and a peak-to-trough duration ≥0.28 ms were classed as

pyramidal cells, whilst units with an overall firing rate ≥3 Hz and a peak-to-trough duration ≤0.25 ms were classed as interneurons (Ranck, 1973). SWR-triggered raster plots and firing rate histograms were determined for each cell (using the SWR onset times determined as above) and the baseline-normalised fold-change in firing rate determined. Cells which changed their firing rate >2 SD from basal firing rates were considered to have significantly responded to the SWR event. The firing phase was determined by linear interpolation between the peaks and troughs of the ripple oscillation, such that the trough of the oscillation was set to 0/360°. The phase profile was only determined for cells which fired at least 40 spikes during the detected ripple oscillations. The Rayleigh test of uniformity ($\alpha = 0.01$) was used to assess the phase distributions for deviations from the circular uniform distribution. A circular concentration gradient, $\kappa$, was used to determine the extent of phase locking (Siapas & Wilson, 1998).

### Statistical analyses

Statistical analyses were performed in SPSS (IBM), Origin 9.0 (OriginLab, Northampton, MA, USA) or Matlab. Data sets were tested for normality using the Shapiro-Wilk test and parametric or non-parametric tests were used as appropriate, with an $\alpha$ level of 0.05. Where appropriate, two-way analysis of variance (ANOVA) was used when comparing datasets across multiple levels. Subsequently, *post hoc* pairwise comparisons were performed using a Bonferroni correction for multiple comparisons. Circular statistics (circular mean, $\kappa$ and Rayleigh test of uniformity) were calculated using a circular statistics tool box for Matlab (Berens, 2009; available at http://www.mathworks.com/matlabcentral/fileexchange/10676-circular-statistics-toolbox–directional-statistics-). Where appropriate, the degrees of freedom for a given *t* statistic are reported in subscript.

### Results

To study how SWRs are disrupted by tauopathy, we surgically implanted tetrodes into the CA1 region of the hippocampus of six WT and seven rTg4510 mice. Over a period of several days post surgery, the tetrodes were lowered to target s. pyramidale; successful arrival at the appropriate anatomical location was indicated online by the appearance of ripple events during peri-ods of restfulness and by *post hoc* histological analysis of the tetrode tracts. Recordings lasting >60 min were performed while mice were allowed to rest and sleep naturally in their home cage. Data were divided into 30 s epochs and those associated with sleep and/or QR were identified using quantitative criteria (see
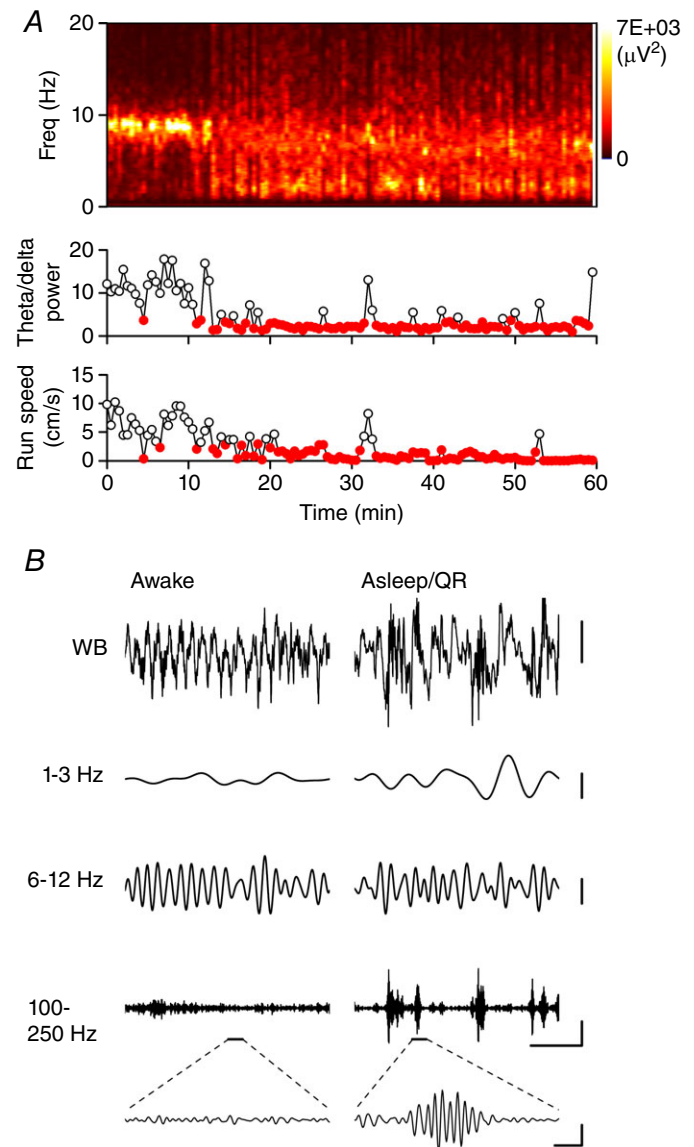
**Figure 1. Isolation of sleep/QR epochs from tetrode recordings made from the CA1 pyramidal cell layer**
*A*, spectrogram showing the spectral profile of LFP activity recorded from a single tetrode wire positioned in s. pyramidale of CA1 in a WT mouse, during a 60 min home cage recording session. The theta/delta power ratio and average movement speed for 30 s time epochs are plotted on the graphs below. Note that as the animal became behaviourally inactive, the theta power decreased whilst the delta power increased. Time epochs which meet the criteria for a sleep/QR epoch (run speed <4 cm s$^{-1}$ and theta/delta power ratio <4) are shown as filled symbols. *B*, example wide-band (WB) and band-pass filtered (in the delta, theta and high frequency ranges) traces (2 s duration) from the same recording session shown in *A*. Example traces are shown from time points where the animal was in an awake, behaviourally active state and in an asleep/QR state. Note the appearance of brief periods of high frequency activity during sleep/QR. A single ripple event is illustrated by the expanded section of the high frequency filtered trace. Scale bars: 500 $\mu$V, 0.5 s for the WB traces and 300 $\mu$V for the filtered traces. Expanded trace scale bar: 200 $\mu$V, 20 ms.

Methods; Fig. 1*A*). Comparison of the s. pyramidale LFP recorded either during active exploration or sleep/QR revealed qualitatively and quantitatively distinct waveforms. During active exploration, a prominent theta frequency (6–12 Hz) oscillation was visible both in the wide-band and band-pass filtered traces (Fig. 1*B*). Conversely, during sleep and/or QR periods, locomotor activity reduced, theta power decreased and delta frequency (1–3 Hz) power increased (Fig. 1*A* and *B*). Furthermore, brief bursts of high frequency (100–250 Hz) ripple activity became readily apparent in the band-pass filtered LFP record (Fig. 1*B*).

Ripple events are associated with a prominent voltage deflection (or sharp wave) that is particularly evident in the dendritic layers of the hippocampus (Ylinen *et al.* 1995). However, since our *in vivo* recordings were made in the pyramidal cell layer, little or no voltage deflection

was discernible (Fig. 2*A*), as has been previously reported *in vivo*, but in contrast to *in vitro* brain slice preparations (Maier *et al.* 2009). Therefore, we classified these events as sharp-wave ripples (SWRs). To examine the properties of SWR activity in rTg4510 mice we used an off-line detection algorithm which searched LFP recordings for high frequency SWR events lasting between 30 ms and 1 s (see Methods). Using this approach, we detected 115–928 SWR events per animal during previously identified sleep/QR epochs in six WT and seven rTg4510 mice (Fig. 2*A*). Strikingly, the mean peak-to-peak amplitude of these events was significantly smaller in rTg4510 ($275 \pm 56\,\mu$V; $n = 7$) than WT mice ($598 \pm 64\,\mu$V; $n = 6$, $t_{11} = 3.8$, $P = 0.003$, unpaired *t* test; Fig. 2*B*). However, the mean SWR duration (WT, $104 \pm 43$ ms; rTg4510, $65 \pm 5$ ms; $t_{11} = 1.0$, $P = 0.3$, unpaired *t* test; Fig. 2*B*) and intra-ripple frequency (calculated as the

number of ripple cycles divided by the ripple duration; WT, $153 \pm 3$ Hz; rTg4510, $157 \pm 3$ Hz; $t_{11} = -0.9$, $P = 0.4$, unpaired $t$ test; Fig. 2*B*) were unaffected in the mutant mice. Finally, the mean occurrence of SWRs in rTg4510 mice ($0.15 \pm 0.03$ Hz) was significantly lower than in WT counterparts ($0.28 \pm 0.01$ Hz; $t_{11} = 4.0$, $P = 0.002$, unpaired $t$ test).

Visual inspection of the raw data traces (Fig. 2*A*) revealed a potential disruption in the temporal dynamics of SWR events in rTg4510 mice. To explore this possibility, we performed a time–frequency analysis by generating time-locked (to the SWR onset), normalised, mean short-time Fourier transforms of SWRs (band-pass 100–400 Hz) for each animal (Fig. 2*C*). This analysis revealed that whilst the temporal profile of SWR events in WT mice was relatively monotonic in nature (i.e. the high frequency power increased to a peak at ~20 ms after the onset of the ripple and then fell to basal levels; Fig. 2*Ca* and *D*), the temporal profile of SWRs in rTg4510 mice was more complex. Thus, many events consisted of multiple distinct peaks in high frequency power (Fig. 2*Cb*) and were relatively lower in peak power compared to background noise (Fig. 2*D*). Furthermore, the mean peak frequency of the SWR events was significantly slower in rTg4510 mice ($135 \pm 3$ Hz, $n = 7$) compared to WT mice ($149 \pm 3$ Hz, $n = 6$; $t_{11} = 3.4$, $P = 0.006$, unpaired $t$ test; Fig. 2*D*).
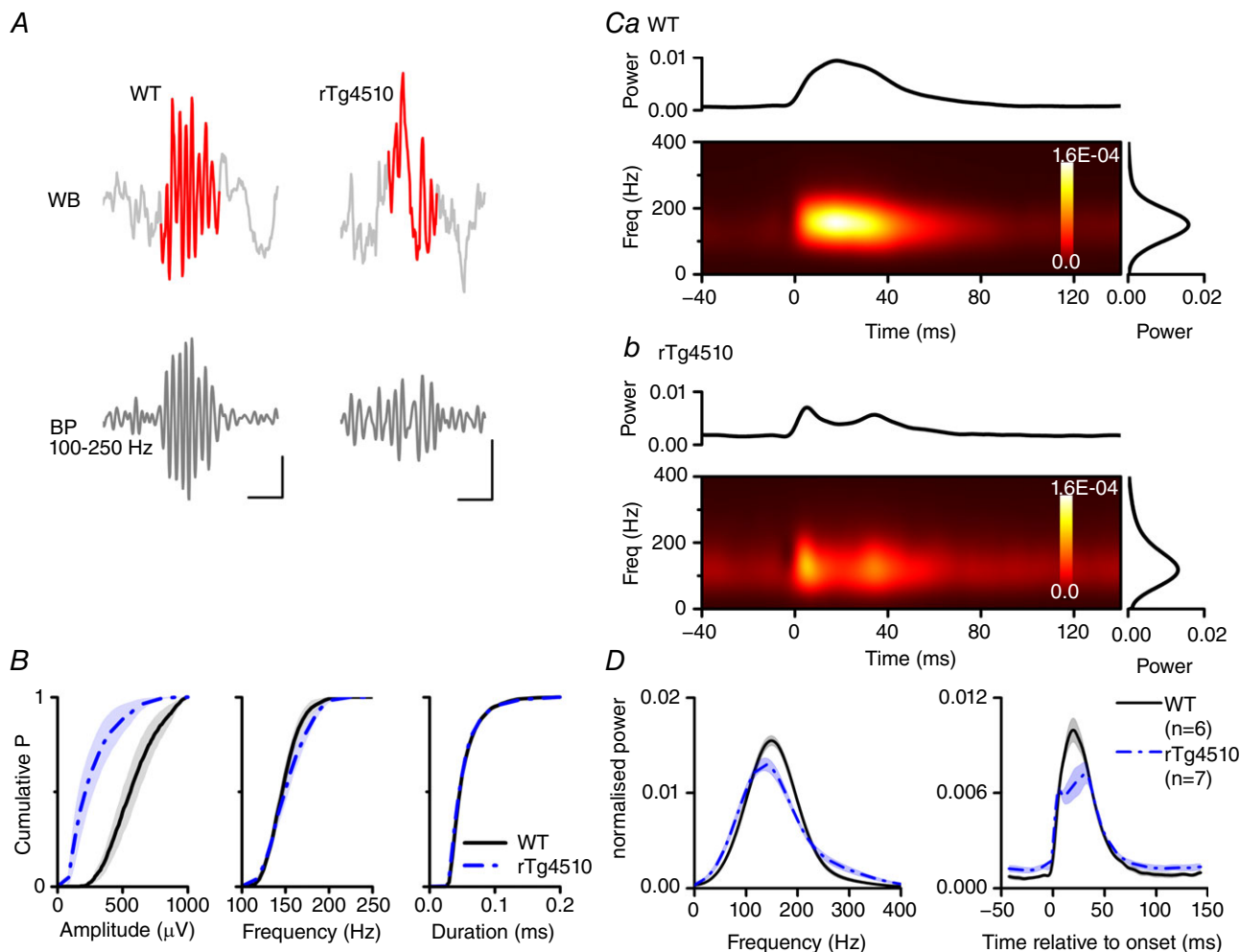


**Figure 2. Amplitude and temporal dynamics of SWR oscillations were disrupted in rTg4510 mice**
*A*, example SWR oscillations detected from LFP recordings made from WT (left) and rTg4510 (right) mice. The detected SWR oscillation is highlighted on the wide-band (WB) trace. The band-pass (100–250 Hz) filtered signal is shown below. Scale bars: WT, 200 μV, 30 ms; rTg4510, 100 μV, 30 ms. *B*, pooled cumulative probability histograms of the SWR event amplitude, frequency and duration in WT (continuous line, $n = 6$ mice) and rTg4510 (dashed–dotted line, $n = 7$ mice) mice. The mean amplitude is significantly lower in rTg4510 mice ($P < 0.05$). *C*, mean normalised short-time Fourier analyses of SWR events recorded from single WT (*a*) and rTg4510 (*b*) mice. The graph above the spectrogram shows the total power with respect to time, whilst the graph to the right shows the total power with respect to frequency. *D*, pooled time-frequency analyses illustrating the significantly lower peak frequency and disrupted temporal profile of SWR events in rTg4510 mice.

Individual neurons within the CA1 region of the hippocampus increase action potential firing rate in a coincident manner with SWRs (Ylinen *et al.* 1995; Klausberger & Somogyi, 2008). Synchronous co-activation of pyramidal neurons during SWRs is thought to drive synaptic plasticity and promote memory consolidation (Sadowski *et al.* 2011), whilst activation of GABAergic interneurons is thought to play a role in generating the SWR event itself (Stark *et al.* 2014). To examine the ripple-associated neuronal dynamics we isolated 120 and 188 single units from the tetrodes in the same six WT and seven rTg4510 mice, respectively. We used standard waveform and firing rate analysis to classify the units as arising from either presumed pyramidal cells or interneurons (see Methods). Using this approach, and given the recording position, the majority of single units (∼70%) were classified as pyramidal cells, whilst ∼5–10% were interneurons. Thus, in WT mice, 81 and

12 were classified as pyramidal cells and interneurons, respectively (Fig. 3), whilst in the rTg4510 mice, 130 and 14 cells were classified as pyramidal cells and interneurons, respectively. 27 and 44 cells, in WT and rTg4510 mice, respectively, fell outside of our classification criteria and were not considered for further analysis (Fig. 3). Qualitatively, presumed pyramidal neurons typically had a bimodal inter-spike interval (ISI) distribution with peaks at 100–200 Hz and 1–10 Hz, whilst presumed interneurons tended to have a more unimodal ISI distribution (Fig. 3). Interestingly, pyramidal cells recorded from rTg4510 mice tended to have a slower overall firing rate when compared with cells recorded from WT mice (WT, $1.12 \pm 0.12$ Hz, $n = 81$; rTg4510, $0.53 \pm 0.05$ Hz, $n = 130$; $P < 0.00001$, Wilcoxon rank sum test). However, mean interneuron firing rates were equivalent between genotypes (WT, $11.3 \pm 1.7$, $n = 12$; rTg4510, $10.4 \pm 1.8$ Hz, $n = 14$; $P = 0.5$, Wilcoxon rank sum test).
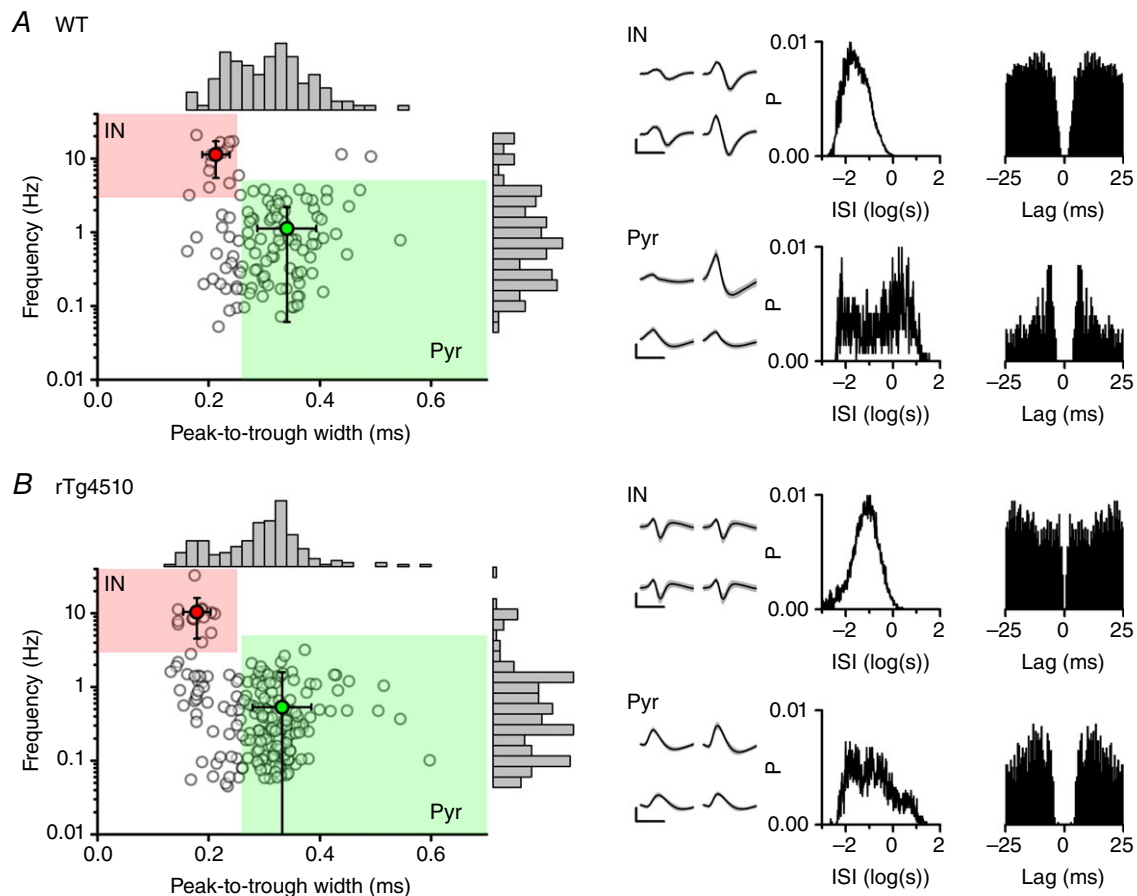


**Figure 3. Classification of isolated single units as presumed pyramidal cells and interneurons**
Scatter plots of the peak-to-trough widths of spike waveforms *vs.* basal firing frequency for all 120 and 188 single units isolated from 6 WT (*A*) and 7 rTg4510 (*B*) mice, respectively. The shaded areas represent the classification criteria for pyramidal (Pyr) and inter-neurons (IN). The means (± SD) of the Pyr and IN groups are also plotted. Marginal histograms for each parameter are shown on the opposing axis. An example interneuron and pyramidal neuron from each genotype are depicted on the right: the mean waveforms from each electrode in a tetrode (± SD shown in grey), the inter-spike interval (ISI) histogram and spike train autocorrelation are shown for each cell.
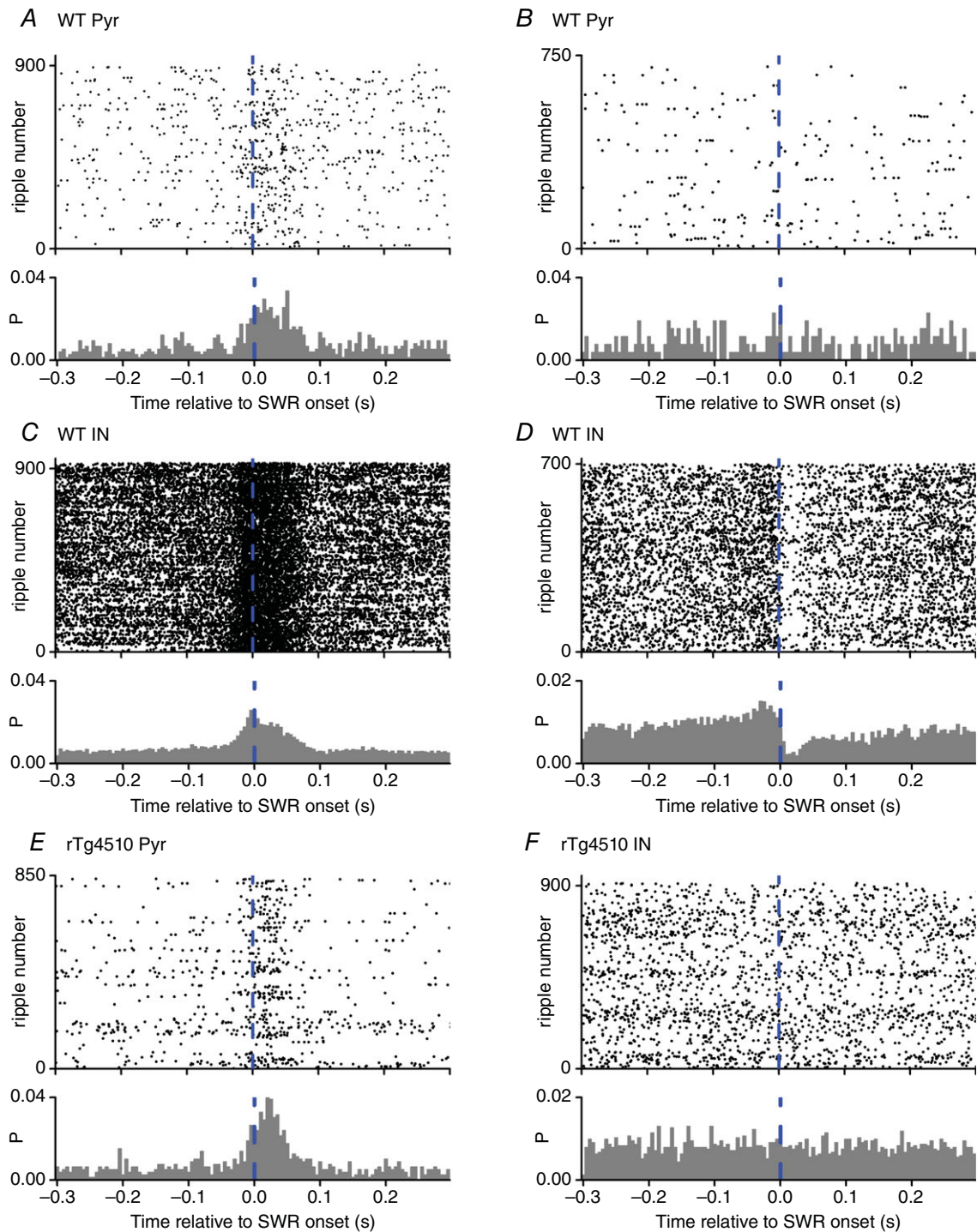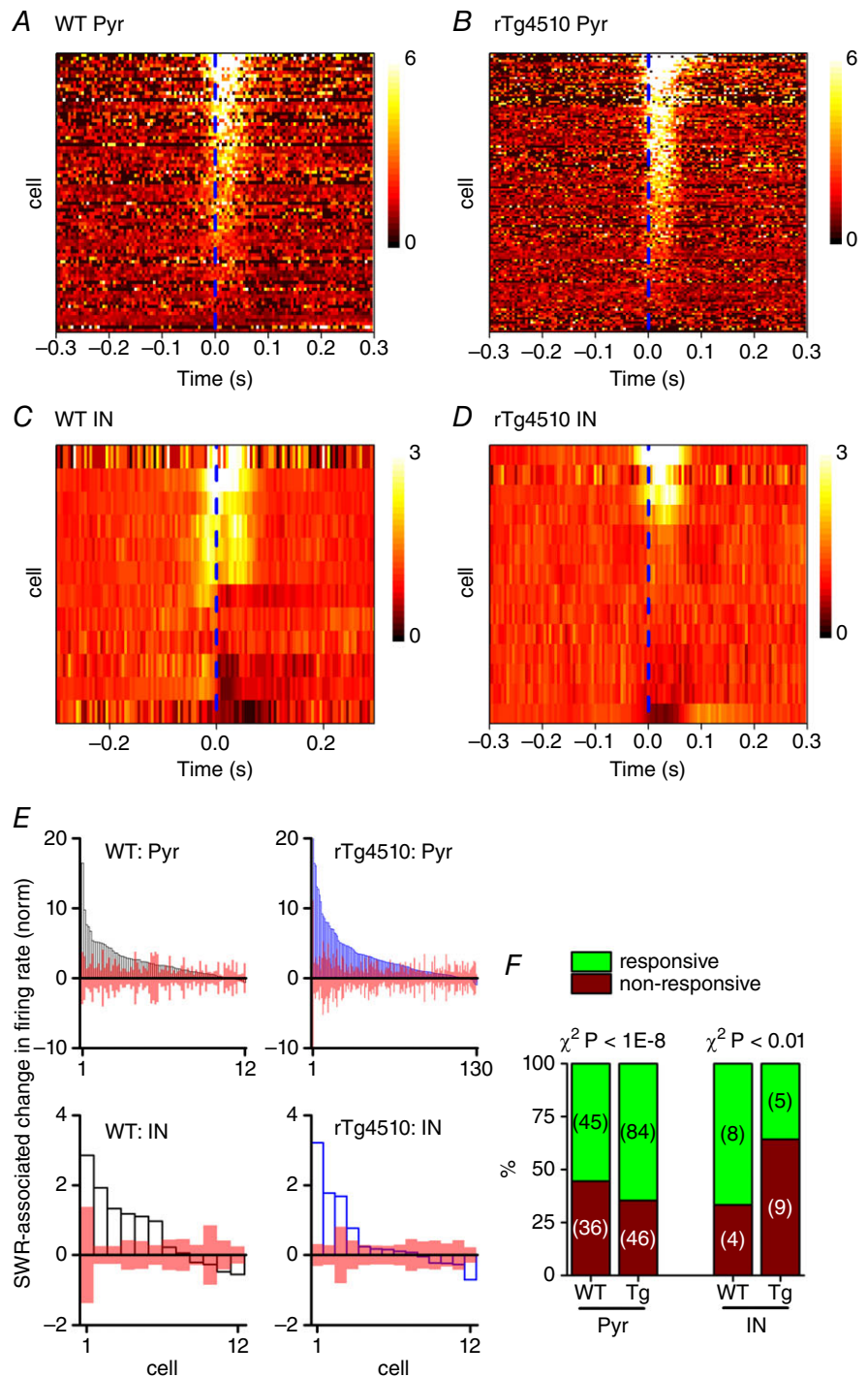
**Figure 4. Firing rates of single units relative to SWR onset**
SWR-triggered raster plots and firing probability histograms for 6 single units. The dashed line represents the onset of the detected SWR events (700–920 per cell). The firing probability histograms were constructed by calculating the probability that a cell fired a spike during a time bin (5 ms bin duration). *A* and *B*, two example WT pyramidal neurons (Pyr) are depicted; one of which was (*A*) and one of which was not (*B*) co-active with the SWR events. *C* and *D*, two example WT interneurons (IN) are shown which increased (*C*) or decreased (*D*) their firing rate. *E* and *F*, examples rTg4510 pyramidal neuron (co-activated with SWR events; *E*) and interneuron (firing rate unaffected by SWR events; *F*).

We next sought to establish whether the change in firing rate associated with SWRs was altered in rTg4510 mice. SWR-triggered raster plots were created for every cell and collapsed to generate firing probability histograms (Fig. 4). Within the pyramidal neuron population there were two types of cells: those that responded to SWR events by significantly increasing their firing rate (Fig. 4*A* and *E*) and those in which the firing rate remained unchanged

(Fig. 4*B*), suggesting that their activity was not influenced by the local SWR events. Changes in firing rate were considered significant if they differed from the normalised basal firing levels by more than 2 SDs of the normalised basal firing rates. No WT pyramidal neurons (out of a total of 87) significantly decreased their firing rate during SWRs and only 1 out of 123 rTg4510 pyramidal neurons significantly decreased its firing rate. Paradoxically, given



**Figure 5. Altered neuronal responsiveness to SWR events in rTg4510 pyramidal cells and interneurons**
*A–D*, pseudocoloured, baseline normalised (baseline = 1) firing probability histograms (see Fig. 4 for examples) of all recorded pyramidal cells (Pyr; *A* and *B*) and interneurons (IN; *C* and *D*). Lighter shades represent increases in firing rates. Cells are sorted according to the magnitude of the change in SWR-associated firing rate. The SWR onset is represented by the vertical dashed line. *E*, peak SWR-associated change in firing rate for each cell (here, baseline = 0, to readily identify neurons which decreased their firing rate). A cell was considered to have significantly responded if the change in firing rate was 2 SD of the basal firing rate (represented by the open bars). *F*, stacked bar graphs illustrating the proportions of cells which significantly altered their peri-SWR firing rate (responsive) and those which did not (non-responsive). A significantly greater proportion ($\chi^2$, $P < 1E-8$) of rTg4510 (Tg) pyramidal cells participated in the SWR events, compared with WT pyramidal cells, whilst significantly fewer rTg4510 interneurons responded to the SWR events ($\chi^2$, $P < 0.01$).

the reduction in amplitude and altered temporal kinetics of SWRs in rTg4510 mice, we found that a significantly greater proportion of pyramidal neurons in rTg4510 mice (65%) significantly increased their firing rate during SWR events, compared to WT pyramidal neurons (56%; $\chi^2$ test, $P < 0.00001$; Fig. 5).

GABAergic interneurons respond to SWR events in a more diverse manner than pyramidal cells (Klausberger *et al.* 2003, 2004, 2005; Le Van Quyen *et al.* 2008). Consistent with these reports, we found that some putative interneurons in WT animals responded with a significant increase in firing rate (Fig. 4C), whilst others responded by substantially reducing their firing rate (Fig. 4D). Interestingly, we found that a significantly lower proportion of interneurons in rTg4510 mice (36%) significantly altered their firing rates in a coincident manner with SWR events, compared to WT interneurons (75%; $\chi^2$ test, $P < 0.01$; Fig. 5).

Examination of the population firing rate histograms revealed that, in WT mice, putative interneurons often fired earlier relative to the SWR onset than pyramidal neurons, indeed often prior to the onset of the detectable ripple waveform in the LFP (Fig. 5A and C). Units which significantly responded to SWR events (using the same criteria as above) were isolated and the timing of their peak firing response was plotted against the mean change in firing rate during the SWR events (Fig. 6). To test these observations statistically we performed a factorial ANOVA. This revealed a significant interaction between genotype and cell type ($F_{1141} = 9.55$, $P = 0.002$), which was interrogated using *post hoc* pair-wise comparisons for simple main effects (Bonferroni adjusted for multiple comparisons). These analyses illustrate that, on average, WT interneurons fire significantly earlier ($-10.6 \pm 0.7$ ms relative to SWR onset, $n = 8$) than WT pyramidal neurons ($+12.9 \pm 0.3$ ms relative to SWR onset, $n = 48$; $P = 0.001$; Fig. 6A and C). These data confirm findings in rats (Klausberger *et al.* 2004) and humans (Le Van Quyen *et al.* 2008), and suggest that interneurons play a key role in controlling SWR dynamics.

In contrast, interneurons which were significantly co-active with SWRs in rTg4510 mice fired later during the SWR event, such that their peak firing time ($+21.0 \pm 0.7$ ms relative to SWR onset, $n = 5$) tended to coincide with, or even follow, the peak firing time of pyramidal cells in these mice ($12.4 \pm 0.2$ ms relative to SWR onset, $n = 84$; $P = 0.3$; Fig. 6B and D). Furthermore, the peak firing time of interneurons in rTg4510 mice was significantly later than in WT mice ($P = 0.002$), whereas pyramidal cell peak firing time was unaffected by genotype ($P = 0.9$).

The spike timing of individual pyramidal cells and interneurons within CA1 is known to be tightly coupled to the phase of the ripple waveform, such that the majority of pyramidal cells and several (but not all) classes of interneuron fire close to the trough of the high frequency oscillation (Le Van Quyen *et al.* 2008; Stark *et al.* 2014). Analysis of the timing of individual units relative to the phase of the ripple oscillation revealed a similar profile in WT cells in this study. Phase histograms were constructed for each cell which fired a total of $\geq 40$ spikes across the SWR events recorded during a session (see Fig. 7A–D for examples). The Raleigh test statistic was used to determine whether the distributions were significantly directional (i.e. 'non-circular'). Furthermore, the extent of phase locking was established by calculating a circular concentration gradient, $\kappa$. The majority of WT pyramidal neurons (33/55 cells, 60%) displayed significant phase locking (Raleigh test, $P < 0.01$) to the ripple oscillation waveform (mean $\kappa = 0.56 \pm 0.04$, $n = 55$; Fig. 7A, E and F). The mean preferred firing phase of WT pyramidal neurons was just prior to the trough of the ripple oscillation (314°, 95% Cl [301°, 326°], $n = 55$; Fig. 7E). Interestingly, a significantly greater proportion of pyramidal cells recorded from rTg4510 mice (57/78 cells, 73%; $\chi^2$ test, $P = 0.0002$; Fig. 7Fa) were significantly phase locked (Raleigh test, $P < 0.01$) to the ripple oscillations, just prior to the trough of the ripple waveform (335°, 95% Cl [326°, 344°], $n = 78$; Fig. 7E). Furthermore, rTg4510 pyramidal cells had significantly higher mean $\kappa$ values ($0.79 \pm 0.08$, $n = 78$; $t_{131} = -2.4$, $P = 0.02$, unpaired $t$ test; Fig. 7C, E and F) compared to WT cells. This was also the case if we only tested the subpopulation of pyramidal cells which displayed significant phase locking (i.e. those cells in which the phase distribution had a Raleigh test $P$ value $< 0.01$) to ripple waveforms (WT, mean $\kappa = 0.72 \pm 0.05$, $n = 33$; rTg4510, mean $\kappa = 0.99 \pm 0.09$, $n = 57$; $t_{88} = -2.2$, $P = 0.03$, unpaired $t$ test; data not shown).

The majority of interneurons (9/12 cells, 75%) recorded from WT mice also displayed a significant level (Raleigh test, $P < 0.01$) of phase locking to the SWR waveform (mean $\kappa = 0.53 \pm 0.08$, $n = 12$; Fig. 7B, E and G). In line with previous studies (Klausberger & Somogyi, 2008; Stark *et al.* 2014), we found that the preferred firing phase of WT interneurons was more diverse than in pyramidal cells, with some cells preferring to fire just before the trough, whilst others fired immediately after (mean phase, 7°, 95% Cl [327°, 46°], $n = 12$; Fig. 7B and E). In marked contrast, a significantly lower proportion of rTg4510 interneurons were significantly phase locked (4/14 cells, 29%, $\chi^2$ test, $P < 0.001$; Fig. 7Ga). Furthermore, the extent of phase locking was significantly lower in rTg4510 cells (mean $\kappa = 0.15 \pm 0.03$, $n = 14$; $t_{24} = 4.7$, $P < 0.0001$, unpaired $t$ test). Again, the extent of phase locking was also lower in rTg4510 cells if we only examined interneurons which were significantly phase locked (WT, mean $\kappa = 0.67 \pm 0.05$, $n = 9$; rTg4510, mean $\kappa = 0.32 \pm 0.04$, $n = 4$; $t_{11} = 4.0$, $P = 0.002$, unpaired $t$ test; data not shown).

## Discussion

In this study we have examined the properties of sleep/QR-associated SWRs and associated neuronal firing dynamics in a mouse model of tauopathy. Our findings indicate that whilst hippocampal neuronal networks in rTg4510 mice were capable of supporting SWRs, the precise control of neuronal recruitment and temporal profile of SWRs was disturbed.

### Mechanism underlying disrupted SWR activity

The temporal dynamics of SWR oscillations in CA1 are thought to require a temporally precise and correct balance of inhibitory and excitatory synaptic transmission. Perisomatic-targeting interneurons are thought to play a key role in generating SWR activity *in vitro* (Ellender *et al.* 2010). Furthermore, the probability of pyramidal cells participating in SWR activity is tightly controlled by inhibitory synaptic transmission (Bähner *et al.* 2011). These findings suggest that correct excitation of, and connectivity between, hippocampal interneurons is critical for the correct initialisation of SWRs. In this study we have shown that GABAergic interneurons in rTg4510 mice are less likely to participate in SWRs and also display significantly lower levels of phase locking to ripple oscillations. Furthermore, the timing of individual interneuron firing, relative to both the SWR event and pyramidal cell firing, is disturbed in rTg4510 mice. Within this framework, we propose that whilst rTg4510 mice have sufficiently intact pyramidal–interneuron networks to initiate SWRs (albeit at a lower occurrence frequency),

the temporal structure of these waveforms is disrupted due to impaired interneuron recruitment and temporal firing dynamics.

Different classes of hippocampal interneuron (of which there are over 20; Klausberger & Somogyi, 2008) respond to SWRs in different ways (Klausberger *et al.* 2003, 2004, 2005; Stark *et al.* 2014). For example, under anaesthesia, basket cells and bi-stratified cell increase their firing rate whilst axo-axonic and oriens–lacunosum moleculare cells tend to decrease their firing rate during SWRs. Using the methodological approaches taken in this study (i.e. tetrode recordings in freely moving mice), it is not possible to definitively classify discrete subclasses of interneuron. Nevertheless, within the population of WT fast spiking presumed interneurons recorded in this study, we see a similar diversity in firing rate changes (Fig. 5), suggesting that basket, bi-stratified and axo-axonic cell types (subtypes with somata located in the recording location employed here, i.e. the pyramidal cell layer; Klausberger & Somogyi, 2008) participate in, or are at least influenced by, the SWR oscillations. In the rTg4510 mice, both increases and decreases in interneuron firing rate were detected, suggesting that multiple cell types still participate in the SWR events, albeit with altered temporal profiles.

Excitatory synaptic contacts onto certain classes of GABAergic interneuron play a key role in regulating and generating SWRs (Cutsuridis & Taxidis, 2013). For instance, genetic down-regulation of fast excitatory synaptic transmission onto PV+ interneurons in the hippocampus results in enhanced phase locking of CA1 pyramidal cells to ripple waveforms, leading to network hyper-synchronisation (Rácz *et al.* 2009). A recent
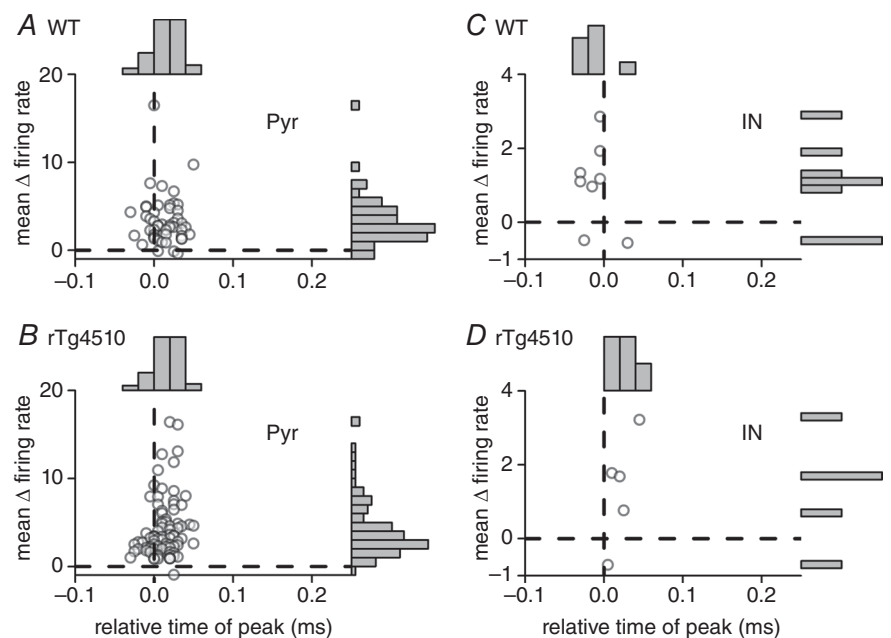


**Figure 6. Altered timing of SWR-associated interneuron firing in rTg4510 mice**

Scatter plots and marginal histograms showing the mean change in firing rate *vs.* relative time of peak change in firing rate for those cells which were significantly co-activated with SWR events. The majority of pyramidal neurons (Pyr; *A*, WT; *B*, rTg4510) responded after the onset of the SWR events. In contrast, the WT interneurons (*C*) tended to fire significantly earlier, prior to the onset of the detectable SWR events, whereas responsive rTg4510 interneurons (*D*) fired significantly later ($P < 0.05$) relative to the SWR events.
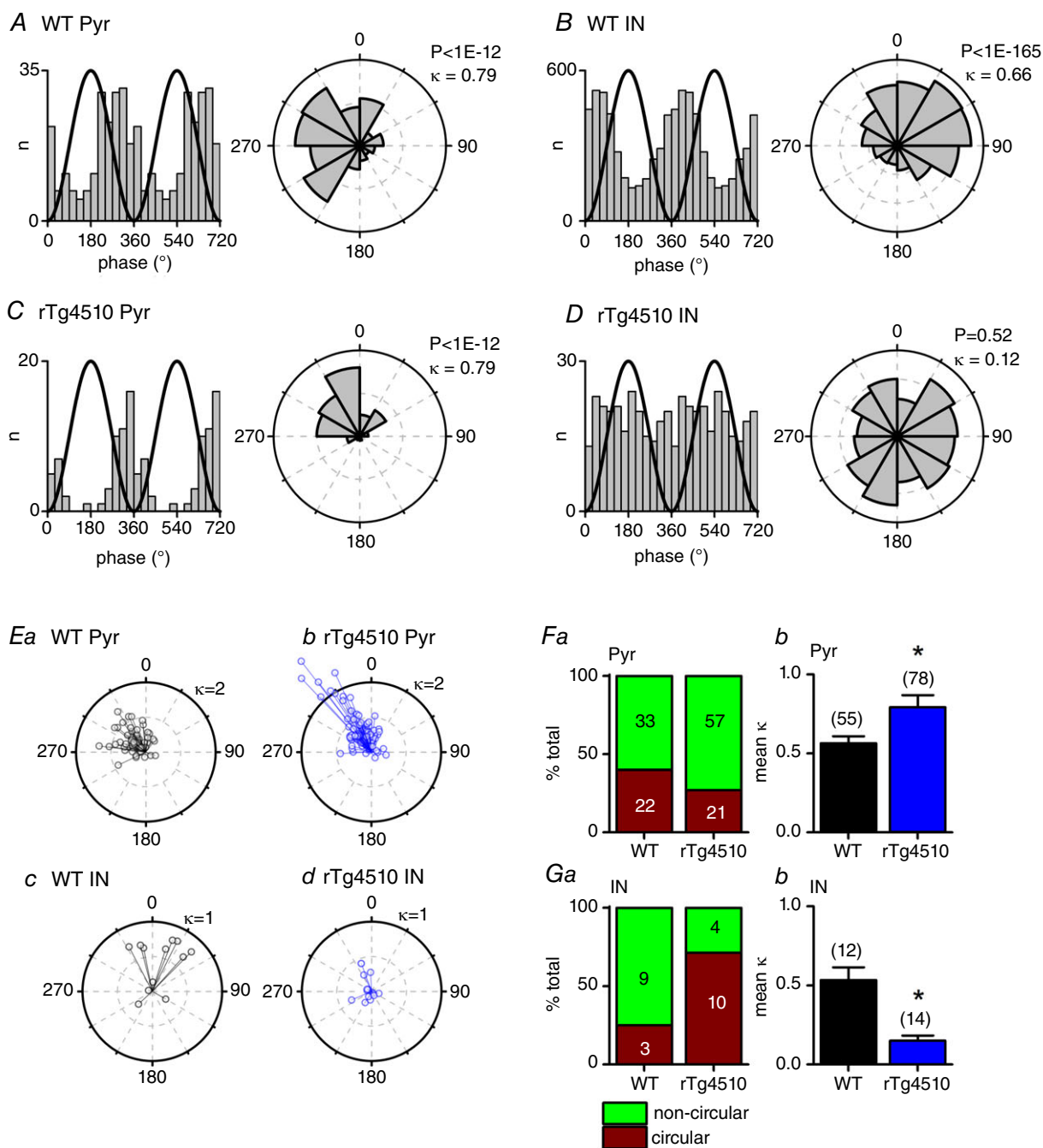
**Figure 7. Altered phase locking of individual rTg4510 neurons to ripple oscillations**
*A–D*, spike phase histograms and corresponding polar histograms, relative to the ripple oscillation phase, for example pyramidal cells (Pyr; *A* and *C*, WT and rTg4510, respectively) and interneurons (IN; *B* and *D*, WT and rTg4510, respectively). A reference line illustrating the ripple waveform phase is plotted in black. For clarity, two ripple cycles are shown. The circular concentration gradient ($\kappa$) and the Raleigh test *P* value are shown for each cell. *E*, the circular mean preferred firing phase of each cell plotted against $\kappa$, for WT pyramidal (*a*), rTg4510 pyramidal (*b*), WT interneuron (*c*) and rTg4510 interneuron (*d*). Both WT and rTg4510 pyramidal cells tended to fire just prior to the trough of the ripple oscillation, whilst WT interneurons fired in a more diverse manner. *F*, a significantly greater proportion of rTg4510 pyramidal cells had significantly non-circular (Raleigh test, $P < 0.01$) firing phase profiles, implying that a greater proportion of cells had firing patterns that were phase locked to the ripple waveform (*a*). The mean $\kappa$ values were significantly (*$P < 0.05$) higher for rTg4510 *vs.* WT pyramidal cells (*b*). *G*, a significantly lower proportion of rTg4510 interneurons had significantly non-circular (Raleigh test, $P < 0.01$) firing phase profiles (*a*). The mean $\kappa$ values were significantly (*$P < 0.05$) lower for rTg4510 *vs.* WT interneurons (*b*).

study has similarly implicated GABAergic interneurons in regulating hippocampal SWRs; pharmacological suppression of inhibition in CA1 using picrotoxin reduced coherence between local, optogenetically evoked SWRs, while optogenetic silencing of PV+ interneurons suppressed spontaneous SWRs and promoted ultra-high frequency oscillations (>200 Hz) (Stark *et al.* 2014), reminiscent of activity observed in the epileptic hippocampus (Bragin *et al.* 1999). Furthermore, picrotoxin-mediated suppression of inhibition in hippocampal slices evokes interictal bursts, during which the majority of CA1 pyramidal neurons are coincidentally activated (Wong & Traub, 1983). Although such ultra-high frequency activity was not observed in our recordings in rTg4510 mice, loss of coordinated excitatory–inhibitory coupling could account for the disrupted temporal dynamics of SWRs and increased recruitment of pyramidal cells to SWRs in rTg4510 mice, and may contribute to the network hyper-synchrony that has been observed in other mouse models of dementia (Minkeviciene *et al.* 2009; Verret *et al.* 2012; Corbett *et al.* 2013).

Furthermore, transgenic manipulations which down-regulate synaptic output from the CA3 region result in a reduced intrinsic ripple oscillation frequency (Nakashiba *et al.* 2009), similar to that observed in this study (Fig. 2). Aspects of these phenotypes are similar to those described in the present study, suggesting that glutamatergic synaptic transmission onto pyramidal cells and interneurons may be disturbed in rTg4510 mice, leading to disruptions in SWRs. In this respect, rTg4510 mice, in common with other mouse models of dementia (Hsia *et al.* 1999; Fitzjohn *et al.* 2001; Brown *et al.* 2005), exhibit disruptions to glutamatergic synaptic structure and function (Hoover *et al.* 2010). Therefore, excitatory synaptic drive from CA3 to CA1 is likely to be deficient, which may contribute to the reduction in overall pyramidal cell firing rates observed in rTg4510 mice (see Results), and, given that CA3-mediated depolarisation of CA1 is purported to drive SWR induction in CA1 (Buzsaki *et al.* 2012; Jefferys *et al.* 2012), may have resulted in the observed reduction in inter-SWR event frequency in rTg4510 mice. However, since SWRs in rTg4510 mice are considerably smaller than WT (Fig. 2), it is also possible that the reduced occurrence of SWRs is a result of poor signal to noise resolution for small events.

## Implications for dementia

The model of dementia used in this study, the rTg4510 mouse (SantaCruz *et al.* 2005), over-expresses a mutant form of tau protein found in fronto-temporal dementia with Parkinsonism, associated with chromosome 17 (Hutton *et al.* 1998). The time course

of the pathological phenotype of this mouse has been well characterised. Tau immunoreactivity in the hippocampus begins as early as 1.5 months old, and is highly prominent by 7–8.5 months (Ramsden *et al.* 2005). Neurofibrillary tangle pathology is evident in these mice at 2.5 months of age, and is extensive by 7 months of age (Spires *et al.* 2006). The tau pathology is also associated with extensive neuro-degeneration, evidenced by a decreased total brain weight at young age points (1–4 months; Ramsden *et al.* 2005) and decreased neuron density throughout the hippocampus (particularly CA1 and dentate gyrus) and cortex (Spires *et al.* 2006). Within CA1, neuron density is reduced by approximately 50% between 5.5 and 7 months of age (Spires *et al.* 2006). Thus, by 7–8 months of age (the age of mice used in this study) rTg4510 mice exhibit substantial neurodegeneration, and as such our findings should be interpreted in this context. Having established that rTg4510 mice of this age have altered SWR activity, it would be valuable to determine if these alterations occur prior to gross neurodegeneration, for example at 4 months of age.

In addition to neuropathological changes, a number of deficits in synaptic connectivity and network activity within the hippocampus have been reported in rTg4510 mice. For example, miniature excitatory postsynaptic currents are significantly smaller and less frequent in neurons cultured from rTg4510 hippocampi compared with WT neurons (Hoover *et al.* 2010). Furthermore, long term potentiation at the CA3–CA1 synapse is reduced in slices prepared from 4.5 month old rTg4510 mice (Hoover *et al.* 2010). Additionally, a recent study has examined hippocampal network activity in awake, behaving rTg4510 mice aged between 7 and 9 months, similar to the ages examined in our study (Cheng & Ji, 2013). The authors report a decrease in the power and frequency of theta oscillations (which dominate the hippocampal LFP during exploratory behaviour) during exploration of open field and linear track environments (Cheng & Ji, 2013). Furthermore, they show the spatially modulated activity of putative CA1 place cells to be severely compromised in rTg4510 mice at this age point (Cheng & Ji, 2013). Interestingly, however, despite the loss of spatial specificity, Cheng & Ji (2013) showed that CA1 pyramidal neurons fired in fixed sequences in rTg4510 mice, regardless of the environment which the mice were experiencing. This observation highlights a level of inflexibility in hippocampal networks in rTg4510 mice and, speculatively, may suggest that surviving CA1 pyramidal neurons in these mice become unable to participate selectively in multiple discrete assemblies whose activity is driven by specific environmental- and/or experience-dependent inputs (Harris, 2005; Buzsáki, 2010). Indeed, the inflexible, sequence-based firing of rTg4510 CA1 pyramidal neurons reported by Cheng and Ji (2013) may, in part, be reflected by the increased participation of these cells in SWR events

in the present study. Taken together, these findings point to large scale reorganisation of hippocampal synaptic networks in this model of dementia.

A number of studies have demonstrated that hippocampal place cell activity is replayed on a compressed time scale during SWR activity (Nádasdy et al. 1999; Lee & Wilson, 2002; Karlsson & Frank, 2009; Davidson et al. 2009), suggesting that these network events facilitate the consolidation of memories. Indeed, online disruption of SWRs by electrical stimulation impairs spatial memory consolidation (Girardeau et al. 2009; Ego-Stengel & Wilson, 2010). Furthermore, the co-incident activation of pyramidal cells during SWRs is thought to drive the induction of synaptic plasticity (Sadowski et al. 2011). In this study we observed that the temporal structure of SWRs was disrupted in rTg4510, but paradoxically, the recruitment and phase locking of pyramidal cells to these SWR events was enhanced.

Erroneous pyramidal neuron firing in SWR events has been reported previously in calcineurin knockout mice, a rodent model of neuropsychiatric disease, although in that study, ripple power and occurrence rates were also enhanced (Suh et al. 2013). In addition, Suh et al. presented evidence that replay of spatial experience during SWR activity was impaired in calcineurin knockouts. In this study, replay of place cell activity was not examined, since the relatively low number of recording tetrodes that we can implant in mice meant that we had insufficient numbers of simultaneously recorded spatially active cells to power such an analysis. Nevertheless, given the impaired GABAergic control of SWRs in rTg4510 mice, it is reasonable to speculate that place cell replay during SWRs, and thus memory consolidation, is disrupted in this model of dementia. In this regard, rTg4510 mice express memory deficits in hippocampal-dependent memory tasks, such as the Morris water maze (SantaCruz et al. 2005; Ramsden et al. 2005).

Alternatively, the enhanced participation of pyramidal cells in SWR events may represent an adaptive response to the synaptic and cellular degeneration that occurs in this mouse model (Ramsden et al. 2005; SantaCruz et al. 2005; Hoover et al. 2010), as in clinical dementia (Braak et al. 1996). As discussed above, rTg4510 mice express substantial neurodegeneration (up 50% cell loss in CA1) at the age point studied here (7–8 months; Ramsden et al. 2005), so the neurons recorded in transgenic mice in this study are, by definition, ones which have yet to succumb to degenerative processes. It is possible that neurons embedded within well-established, active networks are better placed to survive neurodegenerative processes than those which are not. If this were the case, then the remaining neuronal population may be more tightly coupled to ongoing network events, since neurons less well integrated into functional networks would have degenerated.

Hippocampal ripples cannot be readily examined in dementia patients by conventional surface recording techniques such as EEG, due to the deep anatomical location of the hippocampus and filtering of electrical signals by the skull. However, non-rapid eye movement (NREM) slow-wave sleep-associated cortical spindles and hippocampal SWRs are highly synchronous both in rodents (Siapas & Wilson, 1998) and humans (Clemens et al. 2007, 2011), suggesting that coordinated synaptic mechanisms are responsible for their coincident induction. Therefore, cortical sleep spindles may provide a useful surrogate marker for hippocampal SWRs. In this respect, it is noteworthy that clinical Alzheimer's disease has been associated with disturbances to NREM sleep EEG waveforms. In particular, cortical sleep spindles and K-complexes are less numerous and lower in amplitude in patients with dementia (Reynolds et al. 1985). Furthermore, such coordinated interactions between hippocampal and cortical networks are thought to facilitate memory consolidation across distributed cortical engrams (Ji & Wilson, 2007). Impairments in coordinated neural activity have been reported in neurodevelopmental models of neuropsychiatric disease (Phillips et al. 2012), and are thought to lead to some of the cognitive impairments observed in this model (Lodge & Grace, 2009). It would be of great interest to establish whether the disruptions to hippocampal SWRs coincide with impaired cortical spindle–hippocampal SWR synchrony in this and/or other models of dementia.

In summary, we have shown for the first time that hippocampal SWRs are disrupted in a mouse model of dementia. These findings point to a novel cellular network mechanism which may underlie the cognitive impairment observed in dementia.

## References

Bähner F, Weiss EK, Birke G, Maier N, Schmitz D, Rudolph U, Frotscher M, Traub RD, Both M & Draguhn A (2011). Cellular correlate of assembly formation in oscillating hippocampal networks in vitro. Proc Natl Acad Sci U S A 108, E607–E616.

Berens P (2009). CircStat: a MATLAB toolbox for circular statistics. J Stat Softw 31(10), 1–21.

Bokil H, Andrews P, Kulkarni JE, Mehta S & Mitra PP (2010). Chronux: a platform for analyzing neural signals. J Neurosci Methods 192, 146–151.

Braak H, Braak E & Yilmazer D (1996). Pattern of brain destruction in Parkinson's and Alzheimer's diseases. J Neural Transm 103, 455–490.

Bragin A, Engel J, Wilson CL, Fried I & Mathern GW (1999). Hippocampal and entorhinal cortex high-frequency oscillations (100–500 Hz) in human epileptic brain and in kainic acid-treated rats with chronic seizures. Epilepsia 40, 127–137.

Brown JT, Richardson JC, Collingridge GL, Randall AD & Davies CH (2005). Synaptic transmission and synchronous activity is disrupted in hippocampal slices taken from aged TAS10 mice. *Hippocampus* **15**, 110–117.

Busche MA, Eichhoff G, Adelsberger H, Abramowski D, Wiederhold K-H, Haass C, Staufenbiel M, Konnerth A & Garaschuk O (2008). Clusters of hyperactive neurons near amyloid plaques in a mouse model of Alzheimer's disease. *Science* **321**, 1686–1689.

Buzsáki G (2010). Neural syntax: cell assemblies, synapsembles, and readers. *Neuron* **68**, 362–385.

Buzsáki G, Anastassiou CA & Koch C (2012). The origin of extracellular fields and currents EEG, ECoG, LFP and spikes. *Nat Rev Neurosci* **13**, 407–420.

Buzsáki G & Draguhn A (2004). Neuronal oscillations in cortical networks. *Science* **304**, 1926–1929.

Buzsáki G, Horváth Z, Urioste R, Hetke J & Wise K (1992). High-frequency network oscillation in the hippocampus. *Science* **256**, 1025–1027.

Cheng J & Ji D (2013). Rigid firing sequences undermine spatial memory codes in a neurodegenerative mouse model. *Elife* **2**, e00647.

Clemens Z, Mölle M, Eross L, Barsi P, Halász P & Born J (2007). Temporal coupling of parahippocampal ripples, sleep spindles and slow oscillations in humans. *Brain* **130**, 2868–2878.

Clemens Z, Mölle M, Eross L, Jakus R, Rásonyi G, Halász P & Born J (2011). Fine-tuned coupling between human parahippocampal ripples and sleep spindles. *Eur J Neurosci* **33**, 511–520.

Corbett BF, Leiser SC, Ling H-P, Nagy R, Breysse N, Zhang X, Hazra A, Brown JT, Randall AD, Wood A et al. (2013). Sodium channel cleavage is associated with aberrant neuronal activity and cognitive deficits in a mouse model of Alzheimer's disease. *J Neurosci* **33**, 7020–7026.

Csicsvari J, Hirase H, Czurkó A, Mamiya A & Buzsáki G (1999). Fast network oscillations in the hippocampal CA1 region of the behaving rat. *J Neurosci* **19**, RC20.

Cutsuridis V & Taxidis J (2013). Deciphering the role of CA1 inhibitory circuits in sharp wave-ripple complexes. *Front Syst Neurosci* **7**, 13.

Davidson TJ, Kloosterman F & Wilson MA (2009). Hippocampal replay of extended experience. *Neuron* **63**, 497–507.

Ego-Stengel V & Wilson MA (2010). Disruption of ripple-associated hippocampal activity during rest impairs spatial learning in the rat. *Hippocampus* **20**, 1–10.

Ellender TJ, Nissen W, Colgin LL, Mann EO & Paulsen O (2010). Priming of hippocampal population bursts by individual perisomatic-targeting interneurons. *J Neurosci* **30**, 5979–5991.

Fitzjohn SM, Morton RA, Kuenzi F, Rosahl TW, Shearman M, Lewis H, Smith D, Reynolds DS, Davies CH, Collingridge GL & Seabrook GR (2001). Age-related impairment of synaptic transmission but normal long-term potentiation in transgenic mice that overexpress the human APP695SWE mutant form of amyloid precursor protein. *J Neurosci* **21**, 4691–4698.

Girardeau G, Benchenane K, Wiener SI, Buzsáki G & Zugaro MB (2009). Selective suppression of hippocampal ripples impairs spatial memory. *Nat Neurosci* **12**, 1222–1223.

Harris KD (2005). Neural signatures of cell assembly organization. *Nat Rev Neurosci* **6**, 399–407.

Hoover BR, Reed MN, Su J, Penrod RD, Kotilinek LA, Grant MK, Pitstick R, Carlson GA, Lanier LM, Yuan L-L, Ashe KH & Liao D (2010). Tau mislocalization to dendritic spines mediates synaptic dysfunction independently of neurodegeneration. *Neuron* **68**, 1067–1081.

Hsia A, Masliah E, McConlogue L, Yu G-Q, Tatsuno G, Hu K, Kholodenko D, Malenka R, Nicoll R & Mucke L (1999). Plaque-independent disruption of neural circuits in Alzheimer's disease mouse models. *Proc Natl Acad Sci U S A* **96**, 3228–3233.

Hutton M, Lendon CL, Rizzu P, Baker M, Froelich S, Houlden H, Pickering-Brown S, Chakraverty S, Isaacs A, Grover A et al. (1998). Association of missense and 5′-splice-site mutations in tau with the inherited dementia FTDP-17. *Nature* **393**, 702–705.

Jefferys JG, Menendez de la Prida L, Wendling F, Bragin A, Avoli M, Timofeev I & Lopes da Silva FH (2012). Mechanisms of physiological and epileptic HFO generation. *Prog Neurobiol* **98**, 250–264.

Ji D & Wilson MA (2007). Coordinated memory replay in the visual cortex and hippocampus during sleep. *Nat Neurosci* **10**, 100–107.

Karlsson MP & Frank LM (2009). Awake replay of remote experiences in the hippocampus. *Nat Neurosci* **12**, 913–918.

Klausberger T, Magill P & Márton L (2003). Brain-state- and cell-type-specific firing of hippocampal interneurons *in vivo*. *Nature* **421**, 844–848.

Klausberger T, Márton LF, Baude A, Roberts JDB, Magill PJ & Somogyi P (2004). Spike timing of dendrite-targeting bistratified cells during hippocampal network oscillations *in vivo*. *Nat Neurosci* **7**, 41–47.

Klausberger T, Marton LF, O'Neill J, Huck JHJ, Dalezios Y, Fuentealba P, Suen WY, Papp E, Kaneko T, Watanabe M, Csicsvari J & Somogyi P (2005). Complementary roles of cholecystokinin- and parvalbumin-expressing GABAergic neurons in hippocampal network oscillations. *J Neurosci* **25**, 9782–9793.

Klausberger T & Somogyi P (2008). Neuronal diversity and temporal dynamics: the unity of hippocampal circuit operations. *Science* **321**, 53–57.

Lee AK & Wilson MA (2002). Memory of sequential experience in the hippocampus during slow wave sleep. *Neuron* **36**, 1183–1194.

Le Van Quyen M, Bragin A, Staba R, Crépon B, Wilson CL & Engel J (2008). Cell type-specific firing during ripple oscillations in the hippocampal formation of humans. *J Neurosci* **28**, 6104–6110.

Lodge DJ & Grace AA (2009). Gestational methylazoxymethanol acetate administration: a developmental disruption model of schizophrenia. *Behav Brain Res* **204**, 306–312.

Maier N, Morris G, Johenning FW & Schmitz D (2009). An approach for reliably investigating hippocampal sharp wave-ripples *in vitro*. *PLoS One* **4**, e6925.

Minkeviciene R, Rheims S, Dobszay MB, Zilberter M, Hartikainen J, Fülöp L, Penke B, Zilberter Y, Harkany T, Pitkänen A & Tanila H (2009). Amyloid beta-induced neuronal hyperexcitability triggers progressive epilepsy. *J Neurosci* **29**, 3453–3462.

Nádasdy Z, Hirase H, Czurkó A, Csicsvari J & Buzsáki G (1999). Replay and time compression of recurring spike sequences in the hippocampus. *J Neurosci* **19**, 9497–9507.

Nakashiba T, Buhl DL, McHugh TJ & Tonegawa S (2009). Hippocampal CA3 output is crucial for ripple-associated reactivation and consolidation of memory. *Neuron* **62**, 781–787.

Noebels J (2011). A perfect storm: Converging paths of epilepsy and Alzheimer's dementia intersect in the hippocampal formation. *Epilepsia* **52** (Suppl. 1), 39–46.

Palop JJ, Chin J, Roberson ED, Wang J, Thwin MT, Bien-Ly N, Yoo J, Ho KO, Yu G-Q, Kreitzer A, Finkbeiner S, Noebels JL & Mucke L (2007). Aberrant excitatory neuronal activity and compensatory remodeling of inhibitory hippocampal circuits in mouse models of Alzheimer's disease. *Neuron* **55**, 697–711.

Phillips KG, Bartsch U, McCarthy AP, Edgar DM, Tricklebank MD, Wafford KA & Jones MW (2012). Decoupling of sleep-dependent cortical and hippocampal interactions in a neurodevelopmental model of schizophrenia. *Neuron* **76**, 526–533.

Rácz A, Ponomarenko AA, Fuchs EC & Monyer H (2009). Augmented hippocampal ripple oscillations in mice with reduced fast excitation onto parvalbumin-positive cells. *J Neurosci* **29**, 2563–2568.

Ramsden M, Kotilinek L, Forster C, Paulson J, McGowan E, SantaCruz K, Guimaraes A, Yue M, Lewis J, Carlson G, Hutton M & Ashe KH (2005). Age-dependent neurofibrillary tangle formation, neuron loss, and memory impairment in a mouse model of human tauopathy (P301L). *J Neurosci* **25**, 10637–10647.

Ranck JJ (1973). Studies on single neurons in dorsal hippocampal formation and septum in unrestrained rats: I. Behavioral correlates and firing repertoires. *Exp Neurol* **41**, 461–531.

Randall A, Witton J, Booth C, Hynes-Allen A & Brown J (2010). The functional neurophysiology of the amyloid precursor protein (APP) processing pathway. *Neuropharmacology* **59**, 243–267.

Reynolds CF, Kupfer DJ, Taska LS, Hoch CC, Spiker DG, Sewitch DE, Zimmer B, Marin RS, Nelson JP & Martin D (1985). EEG sleep in elderly depressed, demented, and healthy subjects. *Biol Psychiatry* **20**, 431–442.

Sadowski JHLP, Jones MW & Mellor JR (2011). Ripples make waves: binding structured activity and plasticity in hippocampal networks. *Neural Plast* **2011**, 960389.

SantaCruz K, Lewis J, Spires T, Paulson J, Kotilinek L, Ingelsson M, Guimaraes A, DeTure M, Ramsden M, McGowan E *et al.* (2005). Tau suppression in a neurodegenerative mouse model improves memory function. *Science* **309**, 476–481.

Schmitzer-Torbert N, Jackson J, Henze D, Harris K & Redish AD (2005). Quantitative measures of cluster quality for use in extracellular recordings. *Neuroscience* **131**, 1–11.

Selkoe DJ (2002). Alzheimer's disease is a synaptic failure. *Science* **298**, 789–791.

Siapas A & Wilson M (1998). Coordinated interactions between hippocampal ripples and cortical spindles during slow-wave sleep. *Neuron* **21**, 1123–1128.

Simon A, Traub RD, Vladimirov N, Jenkins A, Nicholson C, Whittaker RG, Schofield I, Clowry GJ, Cunningham MO & Whittington MA (2014). Gap junction networks can generate both ripple-like and fast ripple-like oscillations. *Eur J Neurosci* **39**, 46–60.

Spires TL, Orne JD, SantaCruz K, Pitstick R, Carlson G a, Ashe KH & Hyman BT (2006). Region-specific dissociation of neuronal loss and neurofibrillary pathology in a mouse model of tauopathy. *Am J Pathol* **168**, 1598–1607.

Stark E, Roux L, Eichler R, Senzai Y, Royer S & Buzsáki G (2014). Pyramidal cell–interneuron interactions underlie hippocampal ripple oscillations. *Neuron* **83**, 467–480.

Suh J, Foster DJ, Davoudi H, Wilson MA & Tonegawa S (2013). Impaired hippocampal ripple-associated replay in a mouse model of schizophrenia. *Neuron* **80**, 484–493.

Traub RD & Bibbig A (2000). A model of high-frequency ripples in the hippocampus based on synaptic coupling plus axon–axon gap junctions between pyramidal neurons. *J Neurosci* **20**, 2086–2093.

Verret L, Mann EO, Hang GB, Barth AM, Cobos I, Ho K, Devidze N, Masliah E, Kreitzer AC, Mody I, Mucke L & Palop JJ (2012). Inhibitory interneuron deficit links altered network activity and cognitive dysfunction in Alzheimer model. *Cell* **149**, 708–721.

Wong RK & Traub RD (1983). Synchronized burst discharge in disinhibited hippocampal slice. I. Initiation in CA2–CA3 region. *J Neurophysiol* **49**, 442–458.

Ylinen A, Bragin A, Nádasdy Z, Jandó G, Szabó I, Sik A & Buzsáki G (1995). Sharp wave-associated high-frequency oscillation (200 Hz) in the intact hippocampus: network and intracellular mechanisms. *J Neurosci* **15**, 30–46.

## Additional information

### Competing interests

The authors have no competing interests to declare.

### Author contributions

J.W., A.D.R., M.W.J. and J.T.B. conceived and designed the experiments. J.W. performed the experiments and collected the data at the University of Bristol. L.S., U.B. and J.T.B. performed the data analysis. J.T.B. wrote the manuscript with contributions and comments from the other authors. All authors approved the final version of the manuscript.

### Funding

### Acknowledgements